Robotics: Science and Systems 2005
Cambridge, MA, USA, June 8-11, 2005

Modeling Complex Contacts Involving Deformable Objects for Haptic and Graphic Rendering

Qi Luo
IMI Lab, Department of Computer Science
University of North Carolina - Charlotte
Charlotte, NC 28223, USA
qluo@uncc.edu

Jing Xiao
IMI Lab, Department of Computer Science
University of North Carolina - Charlotte
Charlotte, NC 28223, USA
xiao@uncc.edu

***Abstract*— Haptic rendering involving deformable objects has seen many applications, from surgical simulation and training, to virtual prototyping, to teleoperation, etc. High quality rendering demands both physical fidelity and real-time performance, which are often conflicting requirements. In this paper, we simulate contact force between a held rigid body and an elastic object and the corresponding shape deformation of the elastic object efficiently and realistically based on a nonlinear physical model and a novel *beam-skeleton* model, taking into account friction, compliant motion, and multiple contact regions. Our approach is able to achieve a combined update rate of over 1 *k*Hz in realistic, smooth, and stable rendering, as demonstrated by our implemented examples.**

I. Introduction

Modeling deformable objects in contact has been studied both for graphic rendering and for haptic rendering. Early research work on graphic rendering of deformable objects was surveyed by Gibson and Mirtich [1]. More recent survey on graphic and haptic rendering involving deformable objects can be found in [2]. The existing work can be divided mainly into two large categories of approaches: purely geometric approaches (including methods based on splines, patches and free-form geometric models) and physically based approaches (based on mass-spring models and continuum models).

While graphic rendering only needs to make the modeled object deformation *look* realistic, haptic rendering requires that the deformed object *feels* realistic as well, and, comparing to visual images, humans tend to have a more acute, finer, and richer tactile sense of object properties. While the update rate in graphic rendering needs to be around 20–30 Hz to look realistic, the update rate in haptic rendering needs to reach 1 *k*Hz to feel realistic. Therefore, haptic rendering requires much higher level of physical realism and much faster update rate than graphic rendering to achieve high quality and realistic rendering, which is essential for many applications that simulate manipulations in real physical world.

However, high-level of physical realism and fast update rate of rendering are often conflicting requirements. A common approach is to adopt the physically-based deformable models used in graphic rendering, such as mass-spring-damper models and continuum models, and to improve the update rate by applying certain simplifications to speed up computation.

Mass-spring-damper models are rather popular in haptic rendering (e.g. [3][4]). Such models are simple with well understood dynamics, easy to construct and can be used for interactive and even real-time simulation. However, it has drawbacks. The physical accuracy of such a model is often not sufficient. For example, incompressible volumetric objects or thin surfaces that are resistant to bending are difficult to be modeled as mass-spring systems. The model is linear, and in order to simulate nonlinear force response, it is necessary to integrate the linear model in a way similar to using Finite Element Method (FEM), but then real-time update rate for haptic rendering is hard to achieve.

As for continuum models, such as models based on FEM [5], Finite Difference Method [6], Boundary Element Method [7], and Long Element Method [8], real-time performances can be achieved only by further simplifications or adaptive methods. With the aid of pre-calculations and multiresolution methods, deformation of more complicated objects can be simulated in real-time. However, little is done to deal with deformable objects under complex contact states involving multiple contacts and compliant motions with friction, which could make real-time performance hard to achieve. The majority of previous approaches have assumed single contact region and localized deformation [9]. Increasing rendering speed is always at the expense of lowering physical accuracy.

In this paper, we simulate contact force between a held rigid body and an elastic object and the corresponding global shape deformation of the elastic object efficiently and realistically based on a nonlinear physical model and a novel *beam-skeleton* model. Our approach takes into account friction, compliant motion, and multiple contact regions. The objective is both to avoid expensive computation and to preserve physical accuracy of continuum model.

We use the general Duffing equation [10] as a foundation to simulate nonlinear contact forces from a deformed object in contact. The Duffing equation is one of the standard models for studying nonlinear systems subjected to external forces. It is well studied, relatively simple, and yet is powerful to model very complex behaviors [11]. This model is particularly suitable for modeling the nonlinear stiffness of biomaterials, as in surgical simulations. Contact forces of different types of deformable objects (i.e. elastic, plastic, etc) can be simulated

by changing the related parameters, which can be achieved by pre-calculations [9].

We introduce a novel *beam-skeleton* model to compute the stresses and strains of a deformed elastic object at certain extremal points as well as the stresses at multiple contact regions, based on which, we further introduce fast computation of global shape change through an interpolation method that achieves minimization of elastic energy. Moreover, we take into account the different effects of different contact areas on shape change (under the same force).

The rest of the paper is organized as follows. In Section II, we introduce some basic assumptions. In Section III, we briefly describe real-time collision detection used in our approach. In Section IV, V, and VI, we describe our method for contact force modeling and beam-skeleton model for graphic rendering of shape deformation and for dealing with multiple contact region cases. We present some implementation results in Section VII and conclude the paper in Section VIII.

II. Basic Assumptions

Homogeneous Isotropic Elastic Material

Depending on material properties, deformable objects can be categorized into many types. In this paper, we focus on modeling objects that are made of homogeneous isotropic elastic material. The overall deformation effect for such material is nonlinear. However, the nonlinear deformation only exists inside a small neighborhood of the contact point/region where the stress is very high. The stress felt in other regions is much less and can be considered as linearly distributed.

Stable Equilibrium Configurations

We only consider modeling the contact forces caused by quasi-static collision and compliant motion, which means that motions are slow enough such that only deformation occurred at stable equilibrium configurations needs to be considered, where the elastic energy is minimized. This provides an effective discretization of the otherwise continuous force and shape change happened on the elastic object in contact.

Objects and Contacts

We use a mesh model representation for the geometry of the rigid held object. For the elastic object, we maintain both a mesh model and an exact parametric surface model of its undeformed shape (especially if it is non-polyhedral). The exact parametric surface model is used for both fast and accurate computation of shape deformation (Section V).

We define a single *contact region* as a cluster of contact points S such that the distance between a contact point in S and its nearest neighboring contact point in S is less than a threshold r. A contact point outside S is considered belonging to another contact region, and there can be multiple contact regions in general.

We only focus on cases where each single contact region is relatively small so that within the contact region, the first partial derivatives of the originally undeformed surface of the elastic object hardly change. A contact region may consist of just a single contact point.

For any point on the elastic object outside certain immediate neighborhood R of a contact region, we consider its deformation as caused by the stresses and strains spread to it from the contact region as a function of the contact force and call it *global deformation.*

For points inside the neighborhood R of the contact region, we take into account that the shape deformation is not only caused by the contact force but also by the size of the contact region: the greater the size, the smaller the unit pressures are under the same force, and thus the smaller the deformation. We therefore modify the shape deformation inside R accordingly and call the result *local neighborhood deformation* (Fig. 1).

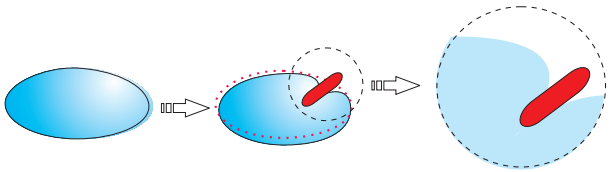

(a) (b) (c)

Fig. 1. Example of shape deformation: (a) originally undeformed elastic object, (b) global deformation over the whole elastic object (the dot line shows the surfaces before deformation), (c) local neighborhood deformation

Force from the Human User

Here we assume that the force exerted to the held object from the human user is applied to the mass center of the held object. This assumption is useful later for estimating the distribution of contact pressure (see Section IV.C).

III. Real-Time Collision Detection

Collision detection for rigid objects has been well investigated. However, real-time collision detection involving a deforming object in interactive environment poses special challenges. Our strategy is to treat contact detection between a rigid body and an elastic object as two rigid bodies at the time of contact and then dynamically change the surface model of the elastic objet to reflect the shape changes due to contacts. Specifically we use a real-time collision detection package SOLID[12] for objects in mesh models that allows dynamic updates of meshes. In each time step i, contact detection is characterized by one of the following three phases.

In the first phase, no contact has yet happened between the two objects, and thus the elastic object does not change its shape. Here collision detection can be considered as just between two rigid objects (in mesh models).

The second phase is marked by the transition from no contact to contact between the two objects, i.e., at least one contact point is established in the current time step i. Once that happens, at least one contact region is formed and recorded.

The third phase describes the situation when the two objects were already in contact in the previous time step $i-1$ and remain in contact in the current time step i, but the contact region(s) may change. There are two possible changes: (1) existing contact region changes because the contact points in it change, and (2) new contact regions are formed. Our contact detection algorithm deals with the situation by comparing the contact points detected in time step $i-1$ with those detected

in the current time step i to update existing contact regions and/or form new contact regions (in terms of mesh models). Note that collision detection can again be treated as between two rigid objects in this phase, but the undeformed shape of the elastic object is replaced by the deformed shape obtained from time step $i-1$.

After all contact regions are determined, contact forces and the corresponding shape change of the elastic object can be computed and rendered haptically and graphically for time step i in real-time as detailed in Sections IV, V, and VI.

IV. Contact Force Modeling for Haptic Rendering

In this section, we first apply the general Duffing equation to provide a nonlinear contact force model for a single point contact caused by pressing the rigid object normally to a face of the elastic object (Fig. 2). Then we extend the method to model other single point contact or single region contact cases.

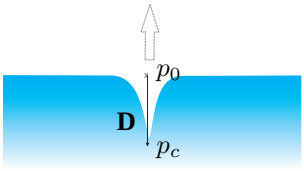

Fig. 2. Contact force simulation: a single point contact with normal compression (the hollow arrow indicates contact force direction)

A. General Duffing Equation

One of the commonly used nonlinear equations for characterizing the behaviors of nonlinear mechanical, electrical and chemical systems is the Duffing equation. We can use the Duffing equation to characterize the nonlinear force response of an elastic object in the basic single point contact case at a quasi-static state as shown in Fig. 2, where p_0 indicates the position of the contact point before deformation, which we call the *origin of the deformation distribution*, and $\mathbf{D}$ is the distance from p_0 to the point of maximum deformation p_c, which we call the *deformation displacement vector* with magnitude D. The Duffing equation essentially defines a nonlinear spring-damper-restorer model.

A general Duffing equation has the following form:

$$\ddot{x} + 2\mu\dot{x} + \omega_0^2 x + \epsilon\beta_0^2 x^3 = A cos\Omega t \tag{1}$$

where x is the deformation distance, $-\omega_0^2 x$ is the linear restoring term, $-2\mu\dot{x}$ is the damping term, $-\epsilon\beta_0^2 x^3$ is the nonlinear restoring term (with $|\epsilon| << 1$), $A cos\Omega t$ is proportional to the external force, and Ω is a constant. Note that the nonlinear restoring force item represents the non-linear properties offered by the deformation of the nearby area.

It is reasonable to assume that the force exerted to the held rigid body from the human operator is constant during one short time step. By using the equivalent frequency ω^* [10], $\omega^* = \omega_0 + 3\beta_0^2 a^2\epsilon/8\omega_0$, where a is the value of x at steady-state, we have the solution as

$$x = e^{-\mu t} C \sin\sqrt{\omega^{*2} - \mu^2}\, t + \frac{A}{\omega^{*2}}$$

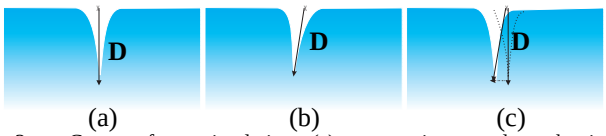

Fig. 3. Contact force simulation: (a) contact is normal to the initial undeformed surface, (b) skewed deformation, (c) compliant motion with deformation

where the first part in the above equation is the transient term and the second part is the steady-state term. With the quasi-static assumption (Sect. II.B), under a large μ, the steady-state is achieved when x reaches D at the end of one time step, i.e.,

$$D = a = \frac{A}{\omega^{*2}} \tag{2}$$

That is, at $x = D = a$, the held rigid object becomes static, and the contact force response $\|\mathbf{F}_c\|$ from the elastic object balances the external force $\|\mathbf{F}_e\| = mA$, where m is the mass of the rigid object. Thus, from (2), by omitting the high order term of ϵ (since $|\epsilon| << 1$), we have

$$\|\mathbf{F}_c\| = m|\omega_0^2 D + \frac{3\beta_0^2\epsilon}{4} D^3| \tag{3}$$

B. Skewed Deformation and Compliant Motion

Now we extend our basic method of contact force simulation to point contact cases where the direction of deformation is not normal to the initially undeformed surface of the elastic object so that the held rigid object may get stuck or perform compliant motion on the elastic object.

When the direction of deformation is not normal to the originally undeformed contact surface of the elastic object (Fig. 3), the deformation displacement vector $\mathbf{D}$ can be decomposed into tangential and normal components $\mathbf{D}_t$ and $\mathbf{D}_n$ respectively. The force response due to deformation along the normal direction $\mathbf{F}_{cn}$ can be computed from (3) with $D = \|\mathbf{D}_n\|$, pointing to the direction against $\mathbf{D}_n$.

Now we need to detect whether the rigid body is stuck or performs a compliant motion tangentially along the contact surface of the elastic object. First, assume that the rigid body is stuck at the current time step i due to the tangential deformation force response from the elastic object $\mathbf{F}_{ct}$, which can be computed from (3) with $D = \|\mathbf{D}_t\|$, pointing to the direction against $\mathbf{D}_t$.

According to [13], the maximum friction from objects of different elasticity is proportional to $\|\mathbf{F}_{cn}\|^\beta$, $\frac{2}{3} \le \beta \le 1$, in the empirical equation $f_{max} = K\|\mathbf{F}_{cn}\|^\beta$ where the coefficient K and β were given in [14] for various deformable materials. For a truly elastic solid, $\beta = \frac{2}{3}$.

Now if $\|\mathbf{F}_{ct}\| \le f_{max}$, our assumption is correct: the rigid object is indeed stuck by the friction so that it will not have a compliant motion at the current time step. Only a skewed deformation happens (see Fig. 3b. Note that the shape of deformation is modeled in Section V). The total contact force response from the elastic object to the rigid body is $\mathbf{F}_c = \mathbf{F}_{cn} + \mathbf{F}_{ct}$.

Otherwise, if $\|\mathbf{F}_{ct}\| > f_{max}$, this represents an impossible case for static friction, indicating that our assumption that the rigid body is stuck is incorrect. On the contrary, the rigid

object in fact makes a compliant motion, which shifts p_0 (i.e., the origin of the deformation distribution) from the previous time step $i-1$ to the current time step i. If the contact point p_c (on the held rigid object) has moved tangentially from time step $i-1$ to time step i with a distance Δd, then to model the effect of compliant motion, we also shift p_0 the distance Δd to obtain its new position. For the dynamic friction $\mathbf{F}_{ct}$, we have $||\mathbf{F}_{ct}|| = \mu_D||\mathbf{F}_{cn}||$ when $\mu_D||\mathbf{F}_{cn}|| < f_{max}$; Otherwise we have $||\mathbf{F}_{ct}|| = f_{max}$, where μ_D is the dynamic friction coefficient. Subsequently, the total contact force response from the elastic object to the rigid body is $\mathbf{F}_c = \mathbf{F}_{cn} + \mathbf{F}_{ct}$. Accordingly, there is a shift of the deformed shape of the elastic object at time step i from that at time step $i-1$ due to compliant motion (as shown in Fig. 3c. See Sect. V for modeling of the shape of deformation).

C. Single Region Contact

A single region contact is formed by a contact region of more than one point. The total effect of contact forces can be obtained by integrating contact forces generated on contact points (or infinitesimal contact areas) over the whole contact region. We discretize the force integration as the summation of contact forces responding to a number of evenly distributed contact points with different displacements of deformation, as shown in Fig. 4. To achieve real-time processing, the discretization can be simply based on the vertex points of the mesh model of the contact region of the rigid object, provided that these vertex points are evenly distributed on the mesh. The contact force response F_i at each contact point p_i can be calculated by the general Duffing equation based on its deformation displacement d_i (Fig. 4) and the mass m_i distributed on it. Summing up all F_i gives the total force F against the direction of deformation **d**.

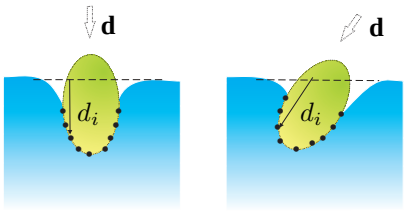

Fig. 4. Examples of single region contact and contact region discretization (**d** is the direction of deformation): (a) normal deformation (b) skewed deformation

In the case of a normal deformation (Fig. 4a), the computed F is *the* total contact force response F_c along the normal of the originally undeformed surface of the elastic object corresponding to the single region contact.

However, in the case of skewed deformation (Fig. 4b), the computed $\mathbf{F}$ with magnitude F along direction $-\mathbf{d}$ should be further decomposed to a normal component $\mathbf{F}_{cn}$ (i.e., normal to the originally undeformed surface of the elastic object) and a tangential component $\mathbf{F}_{ct}$. Depending on the magnitude of $\mathbf{F}_{ct}$, following the same analysis as presented in Sect. IV.B, we can determine whether the held rigid object gets stuck or performs compliant motion as the single region contact occurs and obtain the corresponding total contact force $\mathbf{F}_c$.

Next, we can find an *equivalent point contact* to the single region contact in that the contact force response to that point contact is the same as the total contact force response of the single region contact $\mathbf{F}_c$. With known F_c and m (the mass of the rigid object, which can be considered as concentrated on the equivalent contact point), the equivalent deformation displacement D of the equivalent contact point can be obtained from equation (3). The position of the equivalent contact point p_c before deformation can be considered as at the geometric center of the projection of the contact region on the originally undeformed surface of the elastic object along the deformation direction **d**. See Fig. 5. Using such an equivalence of a point contact to the original single region contact simplifies the shape rendering of the deformed elastic object (see Sect. V).

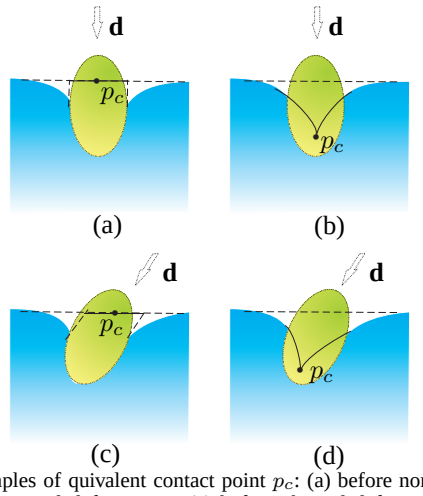

Fig. 5. Examples of quivalent contact point p_c: (a) before normal deformation, (b) after normal deformation, (c) before skewed deformation, (d) after deformation

V. Shape Deformation Modeling and Graphic Rendering

In Sections IV, the contact force response from a contact point or a single contact region of the elastic object to the rigid object is modeled. Now we consider how to model the shape deformation occurred on the elastic object due to such a contact.

A. Global Deformation Modeling and Rendering

Since global deformation is due to the spread of stresses/strains caused by the contact force, in the case of a single region contact, we use the equivalent point contact (which gives the same contact force effect – see Sect. IV.C) to compute the deformation just as in the case of a single point contact, as described below.

Recall that we maintain the exact parametric surface model of the undeformed elastic object (Section II). Because the elastic object without deformation consists of smooth (flat or curved) faces, which may be bounded by smooth (straight-line or curved) edges and vertices, its deformed faces and edges should also be smooth except at bounding vertices and the contact (or equivalent contact) point to minimize elastic energy. Therefore, our strategy to capture the global deformation of an elastic object includes following two steps:

1) Compute the amount of deformation at each curvature extremal point on its boundary surface, which is either a vertex, where the curvature is discontinuous, a point with local minimum or maximum curvature, or an inflection point with zero curvature [15]. These extremal points are obtained from the exact parametric surface model of the elastic object.
2) Do a deformation interpolation between these extremal points and the contact (or equivalent contact) point to obtain smooth deformation of faces and edges of the elastic object.

Both steps can be performed in real time as detailed in the following.

1) Deformation computation at curvature extremal points: To perform the first step, we need to find the elastic force at each curvature extremal point which causes the deformation and compute the amount of deformation accordingly in real-time. For this purpose, we introduce a novel *Beam-Skeleton Model* to capture the underlying physics of elasticity efficiently: once a contact is formed, the stress and strain relations between the contact (or equivalent contact) point and each curvature extremal point on the elastic object is modeled by a beam whose central line connects them, where beam parameters are determined by the physical properties as well as the exact parametric surface properties of the elastic object. The collection of such beams forms what we call a *beam skeleton*. Fig. 6 shows an example of a beam skeleton on an elastic ellipsoid object.

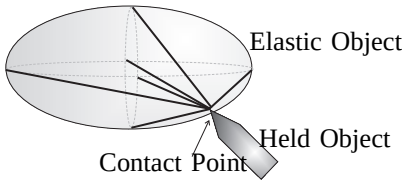

Fig. 6. Beam skeleton (in solid lines) on an elastic ellipsoid object

Now we describe how deformation is computed for a beam of length l (which is determined based on the undeformed shape of the elastic object) bent at one end with the other end fixed based on the Bernoulli-Euler bending beam theory [16]. Establish the beam coordinate system as O-xyz as shown in Fig. 7, where the origin is set at the center point of the fixed end of the beam, and the x axis is along the central line of the beam before it is bent and pointing to the other end of the beam. The y axis is following the bending force direction and the z axis is orthogonal to both the x and y axis following the right-hand rule. A point p on the central line of the beam before it is bent has coordinates $(x, 0, 0)$. Once the beam is pressed at the end that is not fixed, the beam bends, and the new coordinates of p is (x', y', z') satisfying

$$x' = x \qquad y' = \frac{F_y}{EI_z}(\frac{1}{2}lx^2 - \frac{1}{6}x^3) \qquad z' = 0$$

where E is the Young's modules and I_z is moment of inertia with respect to the z axis. At the end of the beam where $x = l$, the relation between the external force F_y normally applied to the beam end and the deformation distance y' is

$$F_y = \frac{3EI_z}{l^3}y' \tag{4}$$

we can relate F_y to the stresses on the beam:

$$\sigma_x = -\frac{F_y}{I_z}(l - x)y \qquad \sigma_y = \sigma_z = \tau_{yz} = 0$$

$$\tau_{yx} = \frac{1}{2(1+\nu)}\frac{F_y}{I_z}[\frac{\partial \phi_1}{\partial y} + \nu z^2 - (1+\nu)y^2]$$

$$\tau_{zx} = \frac{1}{2(1+\nu)}\frac{F_y}{I_z}\frac{\partial \phi_1}{\partial z}$$

where σ's are stresses, τ's are shear stresses, I_z is the moment of inertia, and ϕ_1 is the bending function of the deformable object depending on the shape of the cross section of the beam – for different shapes, ϕ_1 is different.

We call the above case where the external force is normal to the beam a *simple bending case*.

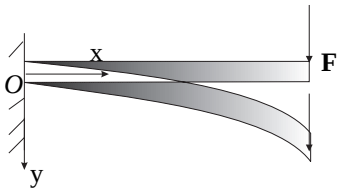

Fig. 7. Schematic of beam bending

In general, the external force applied to a beam at one end is not necessarily normal to the beam central line. In such a case, based on the Saint-Venant principle [17], we can decompose the force into a normal force and a tangential one and decompose the problem of relating the external force to beam deformation into two simpler cases: one is the above simple bending case, and the other is a simple compression/expansion case, which we describe below.

For the simple compression/expansion of the beam caused by a tangential external force F_x, assuming the area of the cross-section of the beam is S, we can relate F_x to the tangential deformation (i.e., compression or expansion) Δx at the beam end $x = l$ with the following equation:

$$F_x = \frac{ES}{l}\Delta x \tag{5}$$

we can also relate F_x to the stresses of the beam:

$$\sigma_x = F_x/S \qquad \sigma_y = \sigma_z = \tau_{xy} = \tau_{xz} = \tau_{yz} = 0$$

The total stresses at a point of a beam are the vector sums of the stresses from the simple bending case and simple compression/expansion case.

In our application, the force **F** applied to a contact or equivalent contact point from the rigid object to the elastic object can be viewed as applied to the common end of a beam skeleton consisting of n beams connecting the common end to each curvature extremal point of the elastic object. The force **F** can be obtained as opposing the contact force response from the elastic object (as computed in Section IV) with the same magnitude. Establish a coordinate frame O_i-$x_i y_i z_i$ for each

beam i ($i = 1, ..., n$) of the beam skeleton such that the origin O_i is located at the i-th curvature extremal point, which is at the other end of the beam i, x_i axis is along the beam central line before it is deformed and pointing to the common end, y_i is on the plane determined by the x_i axis and the force $\mathbf{F}$, and z_i axis is orthogonal to x_i and y_i axes following the right-hand rule.

Now we can view $\mathbf{F}$ applied to the same (contact) point of the common end of all the beams in the skeleton as the sum of the forces $\mathbf{F}_i$ applied to each beam i at the same point so that the deformation occurred at each beam can then be computed separately. Notice that $\mathbf{F}$ does not have a z_i component in the beam i's frame. Let F_{x_i} and F_{y_i} be the x_i and y_i components of $\mathbf{F}_i$. From (4) and (5), we can obtain the following relations among all $\mathbf{F}_i$'s and the relation between each $\mathbf{F}_i$ and the deformation of beam i at the common end of the beam skeleton expressed in beam i's frame:

$$F_{x_1} : ... : F_{x_i} : ... : F_{x_n} = \frac{\Delta x_1}{l_1} : ... : \frac{\Delta x_i}{l_i} : ... : \frac{\Delta x_n}{l_n} \quad (6)$$

$$F_{y_1} : ... : F_{y_i} : ... : F_{y_n} = \frac{y'_1}{l_1^3} : ... : \frac{y'_i}{l_i^3} : ... : \frac{y'_n}{l_n^3} \quad (7)$$

Additionally, the sum of all $\mathbf{F}_i$'s should equal to $\mathbf{F}$:

$$\sum_{i=1}^{n} \mathbf{F}_i = \mathbf{F} \quad (8)$$

From the $2n$ equations (6), (7), and (8), $\mathbf{F}_i$ can be solved for each beam i.

With the above method, we can compute the stresses at the fixed end of each beam (which is centered at a curvature extremal point of the elastic object). Now imagine the fixed end of each beam is no longer fixed, the effect of the stresses will make the corresponding curvature extremal point move to a new position. The position change can be considered as the deformation at such a curvature extremal point, which can be computed from those stresses.

Now we describe how to compute strains from stresses and subsequently compute the deformation at each curvature extremal point. In general, the deformation displacement of a point on the surface of an object can be expressed parametrically as $\{u, v, w\}$, satisfying

$$u = u(x, y, z) \qquad v = v(x, y, z) \qquad w = w(x, y, z)$$

The strain at point (u, v, w) can be represented as

$$\epsilon = \begin{Bmatrix} \epsilon_x \\ \epsilon_y \\ \epsilon_z \\ \gamma_{xy} \\ \gamma_{yz} \\ \gamma_{zx} \end{Bmatrix} = \begin{Bmatrix} \frac{\partial}{\partial x} & 0 & 0 \\ 0 & \frac{\partial}{\partial y} & 0 \\ 0 & 0 & \frac{\partial}{\partial z} \\ \frac{\partial}{\partial y} & \frac{\partial}{\partial x} & 0 \\ 0 & \frac{\partial}{\partial z} & \frac{\partial}{\partial y} \\ \frac{\partial}{\partial z} & 0 & \frac{\partial}{\partial x} \end{Bmatrix} \begin{Bmatrix} u \\ v \\ w \end{Bmatrix} \quad (9)$$

The relation between the strain and stress for a point on a linear elastic object can be represented as

$$\{\epsilon\} = \mathcal{D}^{-1}\{\sigma\} \quad (10)$$

where $\mathcal{D}^{-1}$ is the inverse of the elastic coefficient matrix [16].

Given a curvature extremal point with coordinates $\{x, y, z\}$ and its stresses, we can get its strains from (10). Next, its displacement due to deformation $\{u, v, w\}$ can be solved from these strains using (9).

2) Global deformation rendering: With the displacements of all curvature extremal points of the elastic object due to deformation determined together with the displacement of the contact (or equivalent contact) point, we obtain the deformed shape of the entire elastic object by an interpolation method extending the Phong shading method [18]. Phong shading is used for linear interpolation of vectors at vertices bounding a polygon across internal points of the polygon.

In our case, however, the elastic object can have a general surface with curved features with or without deformation. Let P be the set of curvature extremal points plus the contact point of the surface of the elastic object before the current deformation, note that the elastic object can already be deformed before the current deformation to further change its shape. Such a surface can be partitioned by curves connecting each pair of points in P into smooth curvature-monotonic surface patches, called *faces* [15]. The vertices of each face are a subset of points in P. Now given the deformation displacement vectors of these vertices for each face, we extend the Phong shading to obtain a linear interpolation of the deformation displacement vectors across the face as the following:

> Let θ_i denote the angle between the direction of displacement and the outward normal direction of point i on the face, called the *displacement angle* of point i; the directions of displacement vectors across the face are obtained by linearly interpolating the displacement angles of the vertices of the face, and the magnitudes of displacement vectors across the face are obtained by linearly interpolate the displacement vectors' magnitudes of the face's vertices.

We obtain the deformed shape of the entire elastic object by performing the above shading on all faces. Note that since we do graphical rendering of an object based on its polygonal mesh approximation, the interpolated points of deformation shading of a face can be simply the corresponding mesh points of the face.

It should be emphasized that using our beam-skeleton model to compute deformation fits the physics of elasticity well. First, according to physics, the stresses/strains are smoothly spread over the elastic object surface and have extremal values on the curvature extremal points. Thus, if we can get the stresses/strains on all extremal points of the deformable object, we can get stresses/strains on any points between these extremal points by interpolations. Second, the deformation displacements at these extremal points with respect to the contact region can be thought of as the combination results of extension/compression, bending and twisting, all of which can be captured by the beam-bending model. The global shape deformation of the elastic object obtained from interpolating these displacements satisfies that the closer a surface point to

the contact point or the equivalent contact point, the greater the deformation and curvature change is at this point.

B. Local neighborhood deformation modeling and rendering

For the cases of a single point contact, there is no need to modify the result of global shape deformation described above in the neighborhood R of the contact point.

For the cases of a single region contact, however, the effect of the contact area on shape deformation in the neighborhood R needs to be taken into account. Since the number of mesh points n in the contact region is proportional to the area of the contact region, we can define a *modification factor* $w = \frac{1}{1+logn}$ to capture the effect of the contact area on deformation: the larger the area, the shallower the deformation. Now, we use a modified equivalent deformation displacement wD (where D is determined in Section IV.C), which is shallower than D, to conduct the same kind of interpolation as in global deformation rendering within the neighborhood R on the globally deformed shape to further modify the shape. The result is the combined effect of global shape deformation with local neighborhood shape modification. Fig. 8 shows two examples of local neighborhood shape deformation caused by a single region contact as modeled by this method.

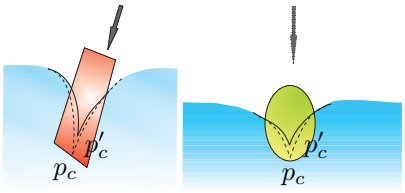

Fig. 8. Two examples of local neighborhood shape deformation (p'_c indicates the modified equivalent point, dotted lines indicate the shapes before modification)

VI. Dealing with Multiple Contact Regions

When there are multiple contact regions (at one time step), $S_i, i = 1, ..., m$, we establish a beam-skeleton model with respect to each contact region in order to compute both the contact force responses and the shape deformation of the elastic object. The beam-skeleton model B_i w.r.t. S_i connects the (equivalent) contact point p_i of S_i to each extremal point of the elastic object as well as the (equivalent) contact point of every other contact region p_j ($j \neq i$) by beams.

The contact force F_{S_i} from the elastic object to the rigid body at contact region S_i consists of not only the force from deformation at S_i alone as described in Section IV but also the stress contributions from every other contact region S_j, ($j \in \{1, ..., m\} - \{i\}$). The stress force contribution from S_j can be computed from the beam-skeleton B_j in a way similar to that described in Section V.A.

The overall shape deformation of the elastic object can be computed by superimposing the shape deformation contributed by each contact region $S_i, i = 1, ..., m$, which can be computed based on each beam-skeleton model B_i in a way similar to that described in Section V. The only difference is that here the (equivalent) contact points p_j's ($j \in \{1, ..., m\} - \{i\}$) are fixed beam ends that do not move so that there is no need to compute strains at those points. Fig. 9 shows an example with two contacts and their beam-skeletons on an elastic ellipsoid.

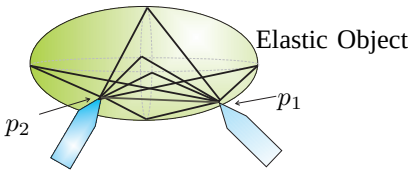

Fig. 9. Beam skeletons for two contacts (in solid lines) on an elastic ellipsoid

VII. Implementation and Test Results

We have implemented our approach and applied it to real-time haptic rendering involving a virtual rigid body and an elastic object via a PHANToM Premium 1.5/6DOF device, which is connected to a computer with dual Intel Xeon 2.4GHz Processors and 1GB RAM. Human operator can virtually hold the rigid object *A* by attaching it to the haptic device and make arbitrary contact to the elastic object *B* (with its bottom center fixed, where a world coordinate system is set) by guarded motions and perform compliant motions on the elastic object. We used the following values for the parameters: $m = 1kg$, $\beta_0^2\epsilon = 0.4$, $\omega_0 = 0.2$, $K = 10$, $\beta = 0.75$, and parameters for rubber: $\rho = 1100Kg/m^2$, $E = 3 \cdot 10^6 N/m^2$, and $\nu = 0.5$.

Figures 10 to 12 show some test results, where the unit of force is Newton, the unit of length is mm, and the unit of time is ms. The world coordinate system in all examples is built as the following: x-axis points right, y-axis points up, and z-axis points out of the paper plane and is orthogonal to x and y axes following the right-hand rule.

Fig. 10 shows a test example with a rigid mallet and an elastic ellipsoid. The human operator first moved down the mallet to make a contact with the elastic ellipsoid, and moved the mallet compliantly along the $+x$ direction mostly and

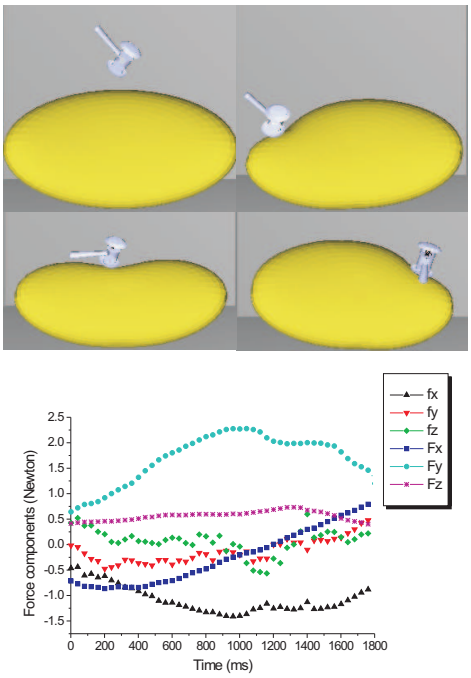

Fig. 10. Force rendering results when a mallet moved compliantly along an ellipsoid

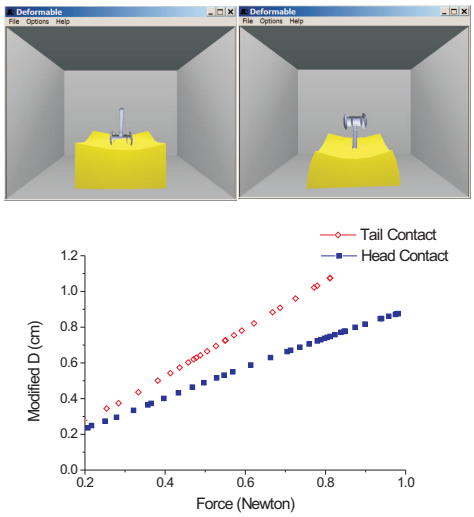

Fig. 11. Comparison of deformation in two different cases of single region contact

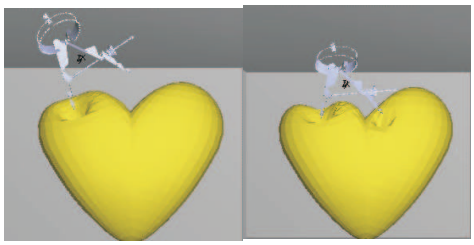

Fig. 12. Two contact regions between a rigid compass and a deformable heart: (left) one contact region (right) two contact regions

slightly toward the $+z$ direction. In this case the contact normal generally has three components: F_x, F_y, and F_z. Here during the compliant motion, the value F_x changed from negative to positive, F_y was always positive and reached the maximum value when the mallet was moved to the upmost position of the ellipsoid, and F_z only had a small positive value since the movement was slightly on the half of the ellipsoid toward the $+z$ direction. For the friction force f_x, f_y, and f_z, f_x always had a negative value since the movement is toward $+x$ direction, f_y increased from negative to positive since the movement was first upward then downward along the y axis, and f_z was almost zero while the oscillation was from the difficulty of moving the mallet in a straight motion.

Fig. 11 shows an experiment to compare the different effects of two cases with different contact areas on local neighborhood shape deformation. In case 1, a mallet's head contacted an elastic cube, and in case 2, the mallet's tail contacted the elastic cube. The contact area in case 1 was larger than the contact area in case 2. We can see that when the same force was applied, the modified equivalent deformation displacement D of case 1 is smaller than that of case 2, which resulted in shallower deformation that fits the related physics principle.

Figure 12 shows example with two contact regions, where a rigid compass first touches a deformable heart with one side pin and then both side pins.

We have used many test examples to confirm the generality of our presented method of computing and rendering contact force and shape deformation. In all of our experiments, modeling and computing haptic force took a constant and almost instant time, of approximately 30 μs, that is, the computation had an update rate of approximately 33 *k*Hz – regardless of the objects geometry. This was negligible compared to the time needed for real-time contact detection (Section III) plus shape updating for the elastic object, which was in the order of *k*Hz. In all test examples shown above, as can be seen, shape deformation of the elastic object looks quite realistic.

VIII. Conclusions

We have introduced a novel approach to model and render in real-time both the nonlinear contact force response and the shape deformation of a general elastic object caused by a rigid object contacting it and moving compliantly on it, taking into account friction. Our approach achieves both real-time efficiency and physical accuracy by taking advantage of nonlinear physics equations, elasticity principles, beam bending theory, and geometrical properties of general surfaces. The approach is implemented to confirm its effectiveness. An update rate of over 1 *k*Hz is achieved for the entire rendering process, including collision detection and rendering both haptic force and graphic shape change. A future research goal is to further test the validity of our approach.

Acknowledgment

This work is partially supported by the National Science Foundation Grants EIA-0224423 and IIS-0328782.

References

[1] S. Gibson and B. Mirtich, "A survey of deformable modeling in computer graphics," TR-97-19, Mitsubishi Electric Research Lab, 1997.
[2] A. Al-khalifah and D. Roberts, "Survey of modelling approaches for medical simulators," in *Proc. 5th Intl Conf. Disability, Virtual Reality and Assoc. Tech.*, (Oxford, UK), pp. 321–329, 2004.
[3] C. Mendoza and C. Laugier, "Simulating cutting in surgery applications using haptics and finite element models," in *VR'03*, pp. 295–296, 2003.
[4] F. Conti, O. Khatib, and C. Baur, "Interactive rendering of deformable objects based on a filling sphere modeling approach," in *Proc. of IEEE Int. Conf.on Robotics and Automation (ICRA)*, pp. 3716–3721, 2003.
[5] S. Laycock and A. Day, "The haptic rendering of polygonal models involving deformable tools," in *EuroHaptics*, pp. 176–192, 2003.
[6] B. Kim and J. Rossignac, "Localized bi-laplacian solver on a triangle mesh and its applications," *GVU Tech. Report: GIT-GVU-04-12*, 2003.
[7] D. James and D. Pai, "A unified treatment of elastostatic contact simulation for real-time haptics," *haptics-e*, vol. 2, no. 1, pp. 1–13, 2001.
[8] K. Sundaraj, C. Mendoza, and C. Laugier, "A fast method to simulate virtual deformable objects with force feedback," in *ICARCV'02*.
[9] M. Mahvash and V. Hayward, "High-fidelity haptic synthesis of contact with deformable bodies," *IEEE CG&A*, vol. 24, pp. 48–55, Feb. 2004.
[10] S. Liu, *Nonlinear Equations in Physics*. Peking Univ. Press, 2000.
[11] L. Miller, "Structural dynamics and resonance in plants with nonlinear stiffness.," *J. Theor. Biol.*, In publication. 2005.
[12] G. Bergen, "Efficient collision detection of complex deformable models using aabb trees," *J. of Graphics Tools*, vol. 2, no. 4, pp. 1–13, 1997.
[13] I. Brown, *Abrasion and Friction in Parallel-lay Rope Terminations*. Ph.D. thesis, University of Cambridge, UK, March 1997.
[14] H. Howell and J. Mazur, "Amonton's law and fiber friction," *Journal of the Textile Institute*, vol. 44, no. 2, 1953.
[15] Q. Luo, E. Staffetti, and J. Xiao, "Representation of contact states between curved objects," in *Proc. of IEEE ICRA*, pp. 3589–3595, 2004.
[16] T. Belytschko, W. Liu, and B. Moran, *Nonlinear Finite Elements for Continua and Structures*. John Wiley and Sons LTD, 2000.
[17] R. Temam and A. Miranville, *Mathematical Modeling in Continuum Mechanics*. Cambridge University Press, 2000.
[18] A. Watt, *3D Computer Graphics*. Addison Wesley, 3rd ed., 2000.